

LETTER TO THE EDITOR

Discovery of HC₉N ν_{19} overtones in IRC+10216

J. R. Pardo^{1,2,*}, J. Cernicharo^{1,*}, J. P. Fonfría¹, C. Cabezas¹, M. Agúndez¹, B. Tercero^{3,4},
N. Marcelino^{3,4}, P. de Vicente³, L. Velilla-Prieto¹, and M. Guélin⁵

- ¹ Departamento de Astrofísica Molecular, Instituto de Física Fundamental (IFF-CSIC), Calle Serrano 121, 28006 Madrid, Spain
² Centre National de la Recherche Scientifique, Observatoire de Paris, LIRA, 77 Avenue Denfert Rochereau, 75014 Paris, France
³ Centro de Desarrollos Tecnológicos, Observatorio de Yebes (IGN), 19141 Yebes Guadalajara, Spain
⁴ Observatorio Astronómico Nacional (OAN, IGN), Calle Alfonso XII 3, 28014 Madrid, Spain
⁵ Institut de Radioastronomie Millimétrique, 300 rue de la Piscine, F-38406 Saint Martin d’Hères, France

Received 7 February 2026 / Accepted 18 March 2026

ABSTRACT

The sub-milliKelvin sensitivity achieved in the Q -band (31–50 GHz) line survey of IRC+10216 obtained with the Yebes 40m telescope reveals the presence of several new vibrational HC₉N overtones ($\nu_{19} \geq 2$) beyond the already reported $\nu_{19} = 1$. The newly found series of rotational lines appears in seven groups with rotational constants (B) between 291.252 and 293.465 MHz, with integer quantum numbers from $J_{\text{up}} = 54$ to 81 and upper-level excitation energies up to ~ 600 K, well above what is typical of lines found in the outer part of this circumstellar envelope. All evidence, especially the spectral splitting of the ℓ -doubling components and the spacing between B values, unambiguously points toward rotational lines within $\nu_{19} = 2$ –8 that appear surprisingly strong, possibly due to very efficient infrared pumping and slow decay via the ν_{19} mode. The detection of $\nu_{19} = 5, 6, 7$, and 8 has been possible thanks to collapsed ℓ -doubling components to a single or only two spectral features per rotational transition. To obtain a correct determination of the abundance of HC₉N in IRC+10216 one has to take into account that about $\sim 70\%$ is estimated to be in the vibrationally excited ν_{19} states.

Key words. line: identification – molecular data – stars: carbon – circumstellar matter – stars: individual: IRC+10216

1. Introduction

One of the main scientific outputs of the ERC synergy project NANOCOSMOS has been an ultra-sensitive Q -band integration on IRC+10216. After a first overall publication presenting spectra accumulated toward this source from May 2019 to February 2020 with the Yebes-40m telescope (Pardo et al. 2022), other specific papers soon followed based on either the same dataset or partial extensions of it completed before 2024 (Pardo et al. 2020, 2021; Changala et al. 2022; Cernicharo et al. 2023a,b; Cabezas et al. 2023). At present, observations have been added until September 2024 with improvements in the receivers, resulting in better system temperatures. The sub-milliKelvin sensitivity in the antenna temperature has led to new findings on the great chemical richness of IRC+10216 (Massalkhi et al. 2024; Gupta et al. 2024; Pardo et al. 2025; Cernicharo et al. 2025).

Several vibrational states of cyanopolyynes have been detected in IRC+10216, including $\nu_{19} = 1$ (Pardo et al. 2020, hereafter P20, and references therein). With this in mind, we have kept our attention on the possible appearance of more energetic ν_{19} overtones and other bending modes of cyanopolyynes as the sensitivity of the IRC+10216 survey increased.

In this work we present the discovery of rotational ladders in previously unreported $\nu_{19} = 2$ –8 bending overtones of HC₉N toward IRC+10216. The data are interpreted in terms of infrared pumping of the vibrational levels of the molecule. We performed a systematic search for all possible bending modes of this species, but only the lowest $\nu_{19} = 1$ and its overtones were

detected. Rotational, distortion, and vibration-rotational spectroscopic constants have been derived for all of these overtones.

2. Observations and analysis

Our recent publication Pardo et al. (2025), hereafter P25, provides the basic information about the observational procedures, technical setup (see also, Tercero et al. 2021), calibration, data accumulation, and reduction. In summary, we achieved 1360 hours of on-source telescope time in 480 observing sessions from April 2019 to September 2024 with the antenna main beam efficiency ranging from 0.60 (31 GHz) to 0.43 (50 GHz); a beam size of 45'' at 39.2 GHz; detection through two HEMT cold amplifiers covering the 31.0–50.3 GHz range; 16×2.5 GHz fast Fourier transform spectrometers used as backends, with a primary spectral resolution of 38.1 kHz (smoothed to 229 kHz for the final data set); and observing mode in position switching, with an off position at 300'' in azimuth. Pointing errors were within 2–3'' and calibration uncertainties within 10%. The global fit strategy using a characteristic line profile for IRC+10216 is described in Section 3 of P25. The experimental results are the integrated areas and the central line frequencies of each individual line returned by a short-iterative process. The horn-to-center intensity ratio, H , from Equation (1) in P25 was kept constant and equal to 0.3 for all lines of interest in this work (other values may apply for lines not important here). With the derived, or fixed in cases of strong blending or poor signal-to-noise ratio (S/N), individual line areas shown in Figure 1, we produced a complete fit spectrum along with rotational diagrams for each relevant spectroscopic species (molecule,

* Corresponding authors: jr.pardo@csic.es;
jose.cernicharo@csic.es

Table 1. Spectroscopic constants (first seven rows) and physical parameters (last two rows) for HC₉N in the ground and eight ν_{19} excited states.

	$\nu_{19} = 0$	$\nu_{19} = 1$	$\nu_{19} = 2$	$\nu_{19} = 3$	$\nu_{19} = 4$	$\nu_{19} = 5$	$\nu_{19} = 6$	$\nu_{19} = 7$	$\nu_{19} = 8$
B (MHz)	290.518317(8)	290.8844(3)	291.2524(7)	291.6231(7)	292.0013(3)	292.3653(5)	292.7245(6)	293.0949(3)	293.4648(4)
α_n (MHz)		0.3661(3)	0.3670(7)	0.3683(7)	0.3707(3)	0.3694(5)	0.3577(6)	0.3681(3)	0.3683(4)
D (Hz)	0.860(7)	0.88(4)	0.90(6)	0.88(5)	0.88(0)	0.88(0)	0.88(0)	0.88(0)	0.88(0)
q (MHz)		0.1463(1)	0.147(13)	0.1458(1)	0.145(4)	0.145(5)	0.139(4)		
X_L (MHz)			1273(18)	1126(17)	1159(58)	1134(11)	1118(54)		
$D_{J\ell}$ (kHz)			-0.33(11)	-0.82(11)	-1.176(35)	-0.62(4)	-0.17(2)		
ρ (Hz)				-1.54(7)	-1.69(3)	-1.55(1)			
T_{rot} (K)	27.5 ± 0.7	30.4 ± 0.9	30.6 ± 2.2	46.0 ± 5.2	45 ± 14	42 ± 19	37 ± 11	57 ± 31	60 ± 35
$N_{\text{col}} \times 10^{-13} \text{ cm}^{-2}$	3.22 ± 0.20	2.10 ± 0.14	1.60 ± 0.26	1.07 ± 0.19	0.59 ± 0.42	0.86 ± 0.45	0.83 ± 0.35	0.28 ± 0.22	0.26 ± 0.22

Notes. For spectroscopy, see text and Yamada et al. (1985). Null uncertainty: Fixed parameter. T_{rot} and N_{col} derived from bottom panel of Fig. 2.

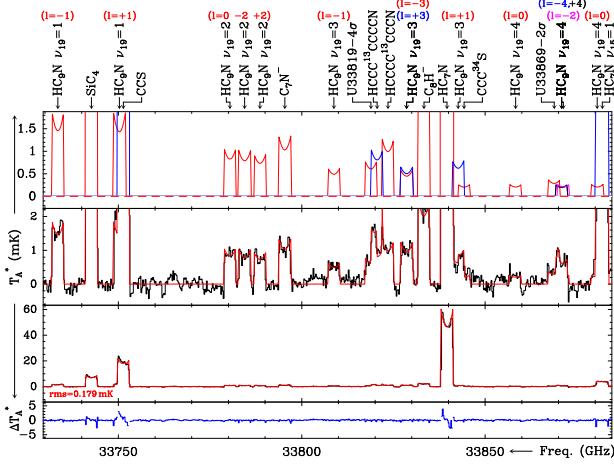


Fig. 1. Example of line identification, decomposition, and fitting of our Q-Band IRC+10216 spectrum around $J_{\text{up}} = 58$ for several HC₉N ν_{19} vibrational states (1,2,3,4) found in this work. The top panel shows individual line contributions (several colors are used to distinguish them if necessary), middle panels show the resulting combination on top of the data, and the lower panel shows fit residuals.

isotopolog, vibrational mode). Examining these diagrams allowed us to identify and correct obviously wrong areas of some blended lines, thus improving the final fit spectrum.

3. Results

For systematic exploration of the data, we used the method described by Cernicharo et al. (2024), which consists of modified Loomis-Wood diagrams (Loomis & Wood 1928). This approach allowed us to explore the data and identify new series of lines that could be assigned to new molecules or to isotopologs and/or vibrationally excited states of known molecules. In each vibrational overtone, $\nu_{19}=n$, each rotational level J has $n+1$ ℓ -doubling components (ℓ from $-n$ to n by steps of 2). Selection rules are $\Delta J = \pm 1$. For $\ell \neq 0$, transitions with $\Delta J=0$ are also allowed (ℓ -doubling transitions). The detection of doublets corresponding to $\nu_{19} = 1$ ($\ell = \pm 1$) was published in P20. Evidence of spectroscopic features compatible with higher ν_{19} states quickly appeared. The $\nu_{19} = 2$ level emerged as a triplet of lines corresponding to $\ell = 0, +2$, and -2 , which are clearly visible in the current dataset (see Fig. 1). With the increase of n , it could be expected that the detectability would rapidly fade as a combination of the higher-level energies and the dispersion of the signal over an increasing number of ℓ -doubling components. However, two facts favor the detection of higher ν_{19} overtones: IR

pumping plays a role in favoring the population of higher vibrational levels, and some ℓ -doubling components collapse to a single feature. In practice, $\nu_{19} = 3$ rotational lines appear as triplets, instead of quartets, because the $\ell = \pm 3$ are closely blended. The same happens with $\ell = \pm 4$ and -2 in $\nu_{19} = 4$. Therefore, we detected a single slightly broadened spectral feature for each J and two separated and weaker features corresponding to $\ell = 0$ and $+2$. For $n=5$, the components with very close frequencies are $\ell = \pm 5$ and $\ell = \pm 3$, and we detected an overlapped doublet. Finally, within $n=6$, the components of the $\ell = \pm 6$ and $\ell = \pm 4$ pairs have each very similar frequencies, and we detected a tighter (compared to $n=5$) overlapped doublet. In the spectral fitting procedure, every single component is entered separately but fit together with its pair. For $\nu_{19} = 7, 8$ only one observed feature per J transition can be assigned to them. We believe that for $\nu_{19} = 7$ we observed four lines at nearly the same frequency corresponding to $\ell = \pm 5$ and $\ell = \pm 7$, and we have assigned one-fourth of the observed area to each one. Similarly, for $\nu_{19} = 8$ the observed features could correspond to a blend of $\ell = \pm 6$ and ± 8 , and the observed area would be split equally among the four. Other ℓ components would be separated in frequency, and therefore, their individual intensity would be too weak for detection.

In order to derive spectroscopic constants (see below) for each ν_{19} overtone, we used a fitting program based on the formalism developed for vibrationally excited bending modes of linear molecules by Yamada et al. (1985) (see also Okabayashi et al. 1999). The fit values were then implemented in MADEX (Cernicharo 2012) to predict the rotational spectroscopy of the overtone. The spectroscopic constants B , D , X_L , and $D_{J\ell}$ in Table 1 correspond to the diagonal contributions to the rotational energy from the rotation and the bending movements, while all the remaining parameters (q and ρ) represent non-diagonal contributions of the bending to the vibration-rotation Hamiltonian. The α_n vibrational constant describes the regular increase in B from one ν_{19} overtone to the next. It is derived as $[B(\nu_{19} = n) - B(\nu_{19} = 0)]/n$ and has an average (giving equal weight to all values) of 0.3682(2) MHz, which is in very good agreement with the value calculated theoretically (~ 0.35 MHz, P20). This gives further support to the identification of the rotational ladders as belonging to ν_{19} overtones. Within the uncertainties, the ℓ -doubling constant q is practically the same, 0.1461(1) MHz, for all vibrational states showing lines with different ℓ components (i.e., from $\nu_{19} = 1$ to 6). This is in excellent agreement with our previous theoretical calculations (~ 0.14 MHz, P20). For $\nu_{19} = 7, 8$ only the rotational constant B could be fit.

We have evidence of 683 rotational transitions from HC₉N, even if not all of these lines are clearly seen individually due to blending between them and/or other species. They represent almost a quarter of all individual lines detected in our survey and

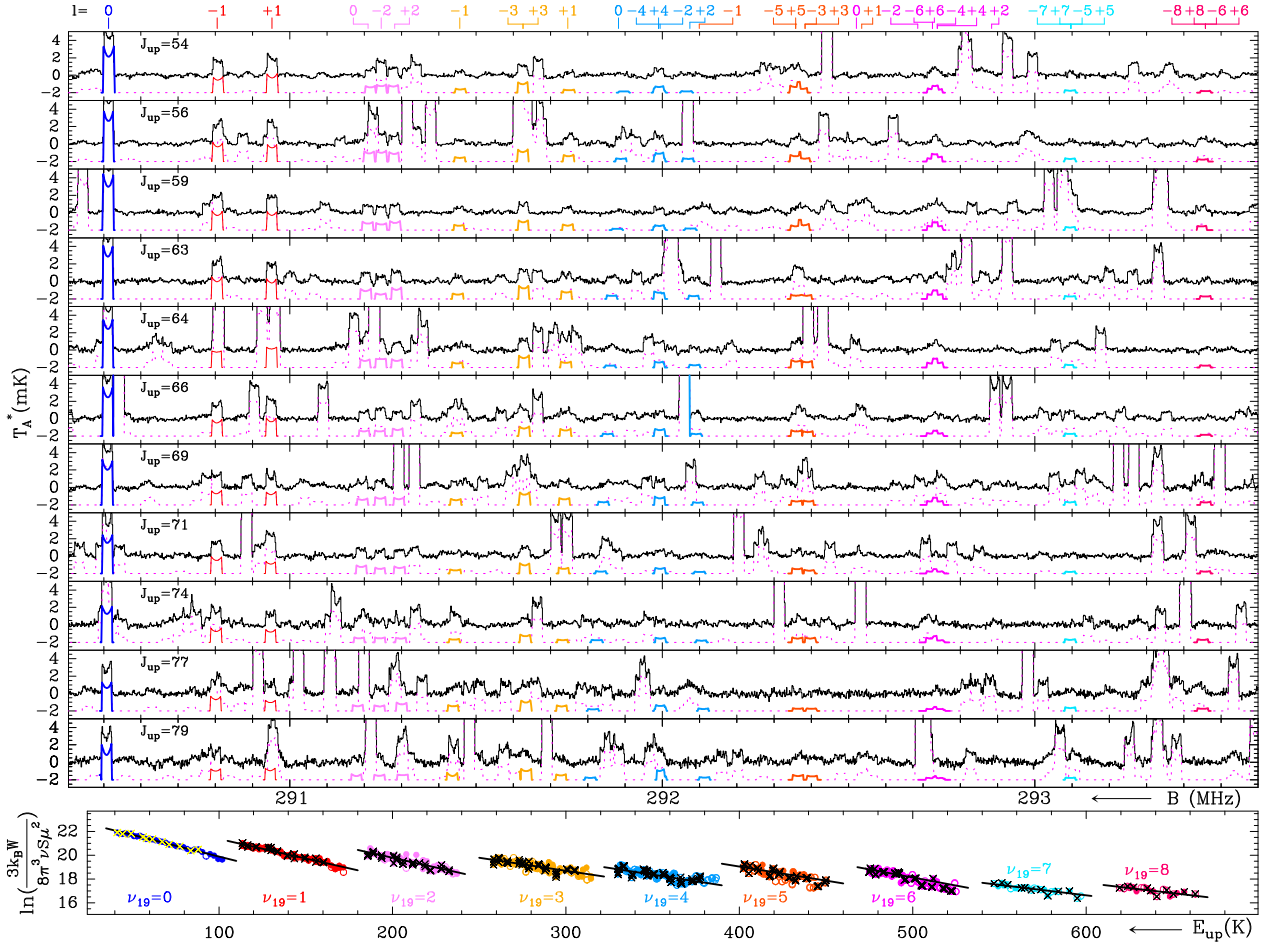


Fig. 2. Top 11 panels: Selected data portions (black histograms) containing HC₉N rotational lines in the ground state, $\nu_{19} = 1$, and seven ν_{19} overtones with their fit contribution highlighted in different colors over the full spectral fit (dotted magenta line shifted by -2 mK). Bottom panel: Rotational diagrams resulting from the HC₉N line areas corrected for beam coupling and dilution over a $30''$ source ($W = \int T_{MB} dv$). Here, μ is the HC₉N electric dipole moment, and S is the quantum line strength of each transition. Filled circles are used for lines with a fit intensity, open circles are for lines with a fixed intensity (due to strong overlap or low S/N), and crosses correspond to the subset of lines actually shown in the top panels. The linear regressions use only the filled circles and provide rotational temperatures and column densities listed in Table 1.

$\sim 33.5\%$ of all lines identified so far. It is obviously impossible to show all HC₉N lines in figures in this Letter, so we have created the compact Figure 2 with selected spectra and the rotational diagrams including points from all observed lines.

4. Discussion

There is clear evidence of a radiative pumping mechanism producing an overpopulation of HC₉N ν_{19} overtones since the typical densities and temperatures of the gas in the circumstellar envelope of CW Leo cannot explain a significant population of the levels involved in the detected transitions, which are well above ~ 600 K in some cases. The rotational temperatures derived from the different rotational ladders are ~ 25 – 45 K, whereas the vibrational temperature would be around 250 K (see values in Table 1 as derived from data in the bottom panel of Figure 2). For the HC₉N ground vibrational state, we can make a rough estimate by using the collisional rates in the MADEX LVG module (Bhattacharyya & Dickinson 1982) and assuming that the emitting gas is in a zone of uniform density and kinetic temperature ($n(\text{H}_2) = 3 \times 10^4 \text{ cm}^{-3}$, $T_K = 25$ K, $N_{[\text{HC}_9\text{N}, \nu_{19}=0]} = 3 \times 10^{13} \text{ cm}^{-2}$) with an expanding velocity $v_{\text{exp}} = 14.5 \text{ km s}^{-1}$, from which we get values of the antenna temperature, after correcting MADEX T_B outputs for the telescope’s efficiency and

dilution over a $30''$ source, that range from ~ 5 mK for $J_{\text{upp}} = 54$ to ~ 2 mK for $J_{\text{upp}} = 79$, which is in reasonable agreement with Figure 2. The rotational diagrams for the ground and the $\nu_{19} = 1$ vibrational state seem to display a curvature due to the decrease of the rotational temperature with increasing J , as expected for any molecule out of local thermodynamic equilibrium, which is already predicted by the above mentioned MADEX LVG calculation. In addition, there is a varying relative contribution of the different circumstellar layers with J that impacts the data. The same effect could be present for $\nu_{19} > 1$, but it is difficult to see due to a low S/N.

In Table B.4 of P20, one can see that the energies of several vibrational states (at least ν_{18} , ν_{17} , and ν_{16}) are below the energy of $\nu_{19} = 6$. Therefore, we should search for them. We have estimates for the spectroscopic parameters, in particular for the rotational constant B and the ℓ -type doubling constant q in Table B.1 of P20. For ν_{18} we should search around the range $B \sim 290.806$ – 290.811 MHz (the upper value being the most possible, as it takes into account a similar correction from predicted to observed as ν_{19}), $q \sim 0.0533$ MHz, and up to ± 0.3 MHz around the resulting positions for the $\ell \pm 1$ components to take into account a wide uncertainty range for B . The parameter q indicates that the splitting into different ℓ components would be smaller (closer in frequency) for ν_{18} than for ν_{19} . The compo-

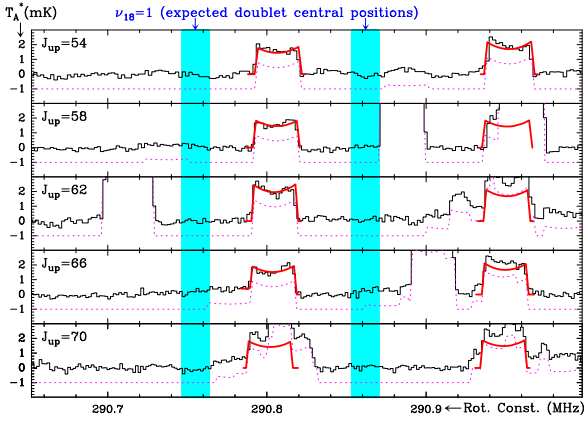


Fig. 3. Expected position (in light blue) for the center of the selected rotational lines within $\nu_{18} = 1$, the lowest vibrational state of HC_9N after $\nu_{19} = 1$ (rotational doublets shown in red), for a selection of J values.

nents would be closer in frequency. In summary, Figure 3 shows the most probable central positions for each component of the $\nu_{18} = 1$ doublets. We did not find coincident spectral features at the given positions, or nearby, that could be related to a rotational ladder within $\nu_{18} = 1$ for the entire range of the explored B . Based on the current sensitivity, the upper limit populations for $\nu_{18,17,\dots} = 1$ is $\sim 10^{12} \text{ cm}^{-2}$.

A qualitative explanation to our data could be that HC_9N absorbs IR radiation in all its stretching (10) and bending (9) modes and their combination bands, chiefly in the range $\lambda \simeq 5\text{--}20 \mu\text{m}$ (see again Table B.4 of P20), where the flux from the source is especially strong and extended. This involves modes $\sim \nu_4$ to ν_{14} and several combinations. The energy of some photons trapped this way ends in a ν_{19} ladder due to a much slower decay rate to the ground state compared to other vibrational modes. Possible (Fermi) resonances between the stretching modes with an overtone n of ν_{19} (or through combination bands) could produce a high population of the $\nu_{19} = n-1$ mode, which is just below the n for which the resonance is produced. Looking to the predicted vibrational frequencies in P20, several cases could be possible. However, precise values of the vibrational energies are needed to make a reasonable argumentation on this mechanism. Direct excitation from the ground to high ν_{19} overtones via far-IR absorption, or collisions with H_2 , would not be efficient enough to reach states beyond $\nu_{19} = 2$. A similar effect, fading with decreasing molecular size, seems to happen for shorter cyanopolynes, as we detect rotational lines within several excited states of their lowest energy bending modes, $\nu_{15} = 1, 2, 3$ (HC_7N), $\nu_{11} = 1, 2$ (HC_5N), and $\nu_7 = 1$ (HC_3N), but not for other modes. A detailed model including all unknown parameters such as ro-vibrational frequencies and radiative and collisional rates remains as a follow-up task.

It is important to point out that the detection of the new ν_{19} vibrational states presented here for the first time, with milliKelvin and sub-milliKelvin antenna temperatures, required several years of data accumulation. IRC+10216 has periodical IR flux variation (see, for example, Shenavrin et al. 2011 and Menten et al. 2012) with a subsequent effect on thermal rotational lines from different species that has been well reported in Cernicharo et al. (2014) and Pardo et al. (2018). The periodic variability is especially well characterized for radicals such as CN, CCH, and C_4H but also, with a lower contrast, for cyanopolynes such as HC_3N and HC_5N . Therefore, it would not be surprising that the newly reported rotational ladders within

the ν_{19} vibrational overtones of HC_9N would also display variability since the populations of these overtones are supposed to be tightly related to this changing IR flux. However, although our spectra span nearly five and a half years (approximately three stellar cycles), a temporal subdivision to search for variability is limited by instrumental changes, irregular temporal sampling, and the requirement to combine all data to reach sufficient sensitivity for $\nu_{19} \geq 2$. A check for the variability of rotational lines on the ground and $\nu_{19} = 1$ states could be done, but this is beyond the scope of this work.

5. Conclusions

We have revealed for the first time the presence of seven new vibrationally (ν_{19}) excited states of HC_9N . However, no other vibrationally excited states ($\nu_{18}, \nu_{17} \dots$) were seen through rotational transitions. We derived the rotational constants for all of the vibrational levels that allow their rotational transitions to be predicted, which should be included in the spectral catalogs used for molecule searches in IRC+10216. A very significant fraction (up to $\sim 75\%$) of the total number of HC_9N molecules in IRC+10216 are in these vibrationally excited states, which is important for the correct determination of the molecular abundances of long carbon chain molecules. We have given possible qualitative explanations for the peculiar presence of so many ν_{19} overtones, but a detailed study would require knowledge of radiative and collisional rates, which are unknown at the present.

Data availability

The complete list of HC_9N transitions identified in this work and the full numerical data used for the bottom panel of Figure 2 are available at the CDS via <https://cdsarc.cds.unistra.fr/viz-bin/cat/J/A+A/709/L13>

Acknowledgements. Based on observations carried out with the Yebes 40m telescope through projects 19A010, 20A017, 20B014 and 21A019, and 23A026. The 40m radio telescope at Yebes Observatory is operated by the Spanish Geographic Institute (IGN; Ministerio de Transportes, y Movilidad Sostenible). We thank the ERC for funding support through grant ERC-2013-SyG-610256-NANOCOSMOS, and to the Spanish “Ministerio de Ciencia, Innovación y Universidades”, FEDER, ESF+ for funding support through the grants PID2020-117034RJ-I00, PID2022-137980NB-I00, PID2023-147545NB-I00, and RYC2023-045648-I (MICIU/AEI/10.13039/501100011033).

References

- Bhattacharyya, S. S., & Dickinson, A. S. 1982, *A&A*, 107, 26
- Cabezas, C., Pardo, J. R., Agúndez, M., et al. 2023, *A&A*, 672, L12
- Cernicharo, J. 2012, *EAS Publ. Ser.*, 58, 251
- Cernicharo, J., Teyssier, D., Quintana-Lacaci, G., et al. 2014, *ApJ*, 796, L21
- Cernicharo, J., Pardo, J. R., Cabezas, C., et al. 2023a, *A&A*, 670, L19
- Cernicharo, J., Cabezas, C., Pardo, J. R., et al. 2023b, *A&A*, 672, L13
- Cernicharo, J., Cabezas, C., Fuentetaja, R., et al. 2024, *A&A*, 690, L13
- Cernicharo, J., Pardo, J. R., Agúndez, M., et al. 2025, *A&A*, 700, L20
- Changala, P. B., Gupta, H., Cernicharo, J., et al. 2022, *ApJ*, 940, L42
- Gupta, H., Changala, P. B., Cernicharo, J., et al. 2024, *ApJ*, 966, L28
- Loomis, F. W., & Wood, R. W. 1928, *Phys. Rev.*, 32, 223
- Massalkhi, S., Agúndez, M., Fonfría, J. P., et al. 2024, *A&A*, 688, A16
- Menten, K. M., Reid, M. J., Kamiński, T., et al. 2012, *A&A*, 543, A73
- Okabayashi, T., Tanaka, K., & Tanaka, T. 1999, *J. Mol. Spec.*, 195, 22
- Pardo, J. R., Cernicharo, J., Velilla-Prieto, L., et al. 2018, *A&A*, 615, L4
- Pardo, J. R., Bermúdez, C., Cabezas, C., et al. 2020, *A&A*, 640, L13
- Pardo, J. R., Cabezas, C., Fonfría, J. P., et al. 2021, *A&A*, 652, L13
- Pardo, J. R., Cernicharo, J., Tercero, B., et al. 2022, *A&A*, 658, A39
- Pardo, J. R., Fonfría, J. P., Agúndez, M., et al. 2025, *A&A*, 700, L6
- Shenavrin, V. I., Taranova, O. G., & Nadzhip, A. E. 2011, *Astron. Rep.*, 55, 31
- Tercero, F., López-Pérez, J. A., Gallego, J. D., et al. 2021, *A&A*, 645, A37
- Yamada, K. M. T., Birss, F. W., & Aliev, M. R. 1985, *J. Mol. Spec.*, 112, 347